La mer 41 : 137–154, 2003
Société franco-japonaise d'océanographie, Tokyo

Flow Analysis of the Arctic Ocean (the Kara Sea and the Barents Sea) by a Hybrid Box Model

Akira WADA* and Minoru OCHIAI*

Abstract : The objective of this report is to discuss the characteristics of flows in the Arctic Ocean Seas (the Kara and the Barents) in connection with marine contamination. In recent years, research has been underway to clarify the fate of radioactive wastes dumped into the Arctic Ocean (especially, the Kara Sea and the Barents Sea) . These sea areas are very narrow, shallow and located close to land. To analyze the diffusion of radionuclides and carry out exposure dose assessment by determining the circulation of seawater in these areas, it is necessary to identify the flow characteristics of the seas. As the first step of research, the mechanism of flows in the Barents Sea and the Kara Sea in the Arctic Ocean was investigated (Local model). Using the observation data (water temperature and salinity) , the flow was analyzed using a hybrid box model, taking into account river flows and density structures in the seas. The results thus obtained agreed with the observed features in many aspects.

Keywords : *Arctic Ocean, Flow analysis, Kara Sea, Barents Sea, Hybrid box model, Local Model*

1. Introduction

Recently, there has been considerable interest in the dumping of radioactive wastes into the Arctic Ocean (especially, the Kara Sea and the Barents Sea) by the former Soviet Union. These seas are narrow, shallow and close to land (see Fig. 1). To assess the impact of such dumping, it is necessary to establish a safety assessment method that permits the prediction of not only regional but also global－scale effects.

To analyze the diffusion of radionuclides and make an exposure dose assessment by determining the circulation of seawater in these areas, it will be necessary to identify the flow characteristics of the seas. However, little research has been conducted insofar as these sea areas are concerned. Moreover, these seas are largely ice－covered in winter, thus available winter oceanographic data are limited. In this research, the authors used existing salinity and water temperature data and information such as meteorological and oceanographical data provided by IAEA.

Representatives of both IAEA and Seven Member states (Danish/Norwegian group, Japan, The Netherlands, The Russian Federation, Switzerland, United Kingdom and United States of America) were involved in the modeling, coordinated within the framework of the IAEA's International Arctic Assessment Project (IASAP). The model and assessment exercises included contributions to all the important aspects required for radiological assessment studies (WADA *et al*., 1997).

This paper centers on flow modeling and its analysis, which is of major significance to assessment exercises. Using these observation data (water temperature and salinity), the wa ter－mass characteristics of the Arctic Ocean were examined with reference to the known data, and the results thus obtained were compared with the results of flow analysis to investigate the present condition of flows in these sea areas.

2. Method of study

What impact will the actual dumping of radioactive waste into the Arctic Ocean have in

* Nihon University, College of Industrial Technology, 1–2–1, Izumi, Narashino, Chiba 275–8575

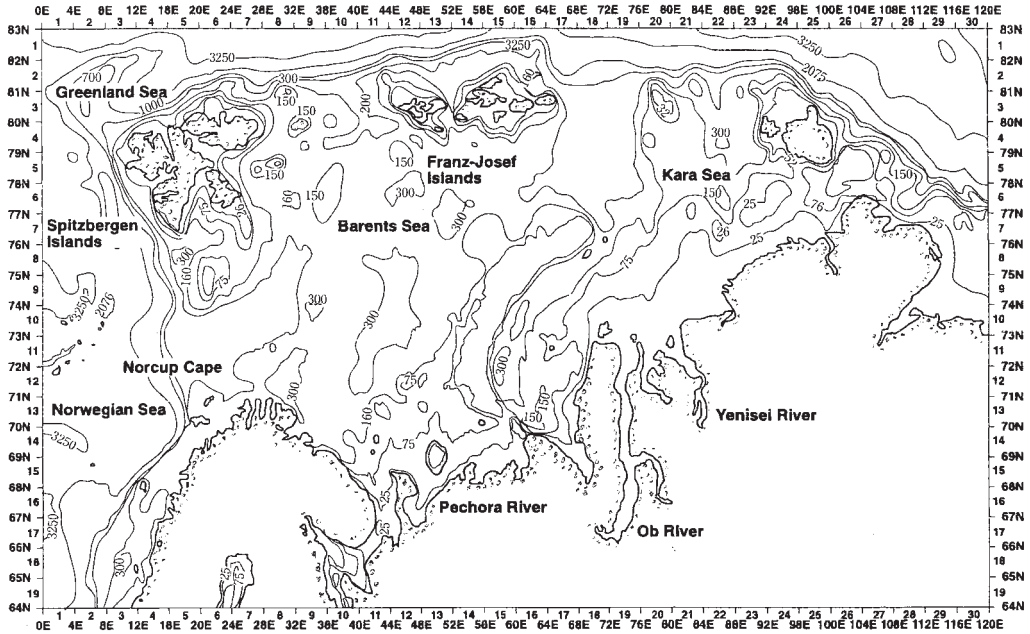

Fig. 1. The Barents Sea and the Kara Sea.

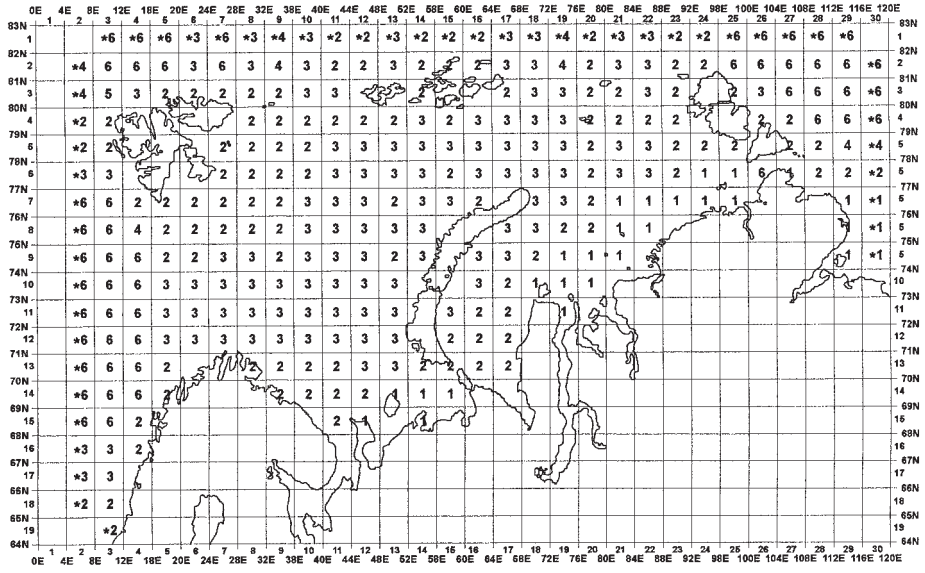

Fig. 2. Grids of the model and the number of vertical layers.

the future? As a first step to solve this question, the authors investigate the flows in the Barents Sea and the Kara Sea based on observed water temperature and salinity distributions in these seas (local scale). Based on data obtained by NOAA's observations (LEVITUS, 1982), water temperature and salinity in the range of 64°–85° N and 0°–120° E were obtained and graphically represented at intervals of 0.1 ℃ and 0.1psu respectively, and were used to examine the oceanographical characteristics of these seas. The horizontal box size was

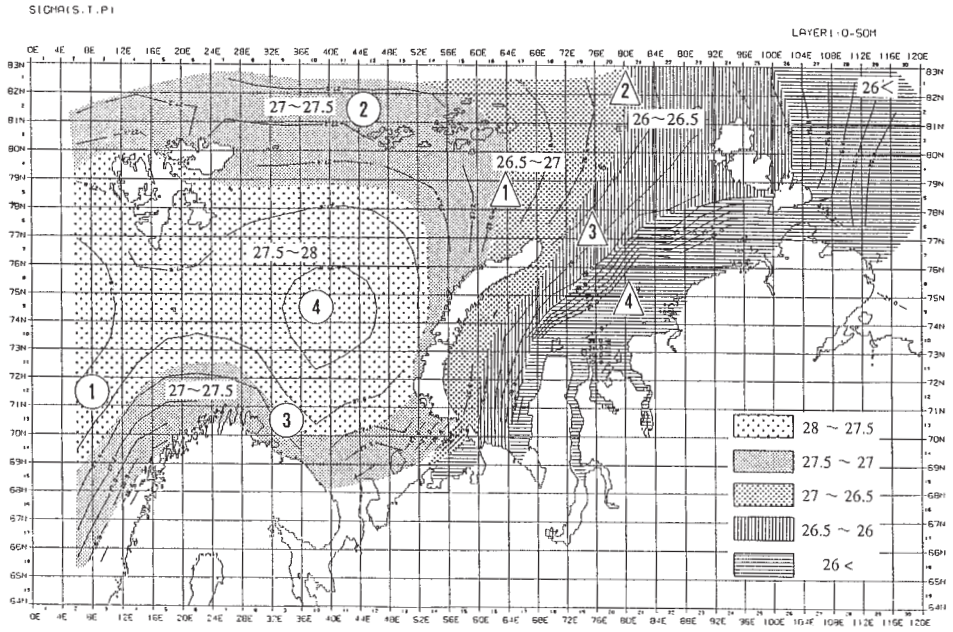

Fig. 3. (1) Density distribution σ_t (0–50m layer, warm weather season).

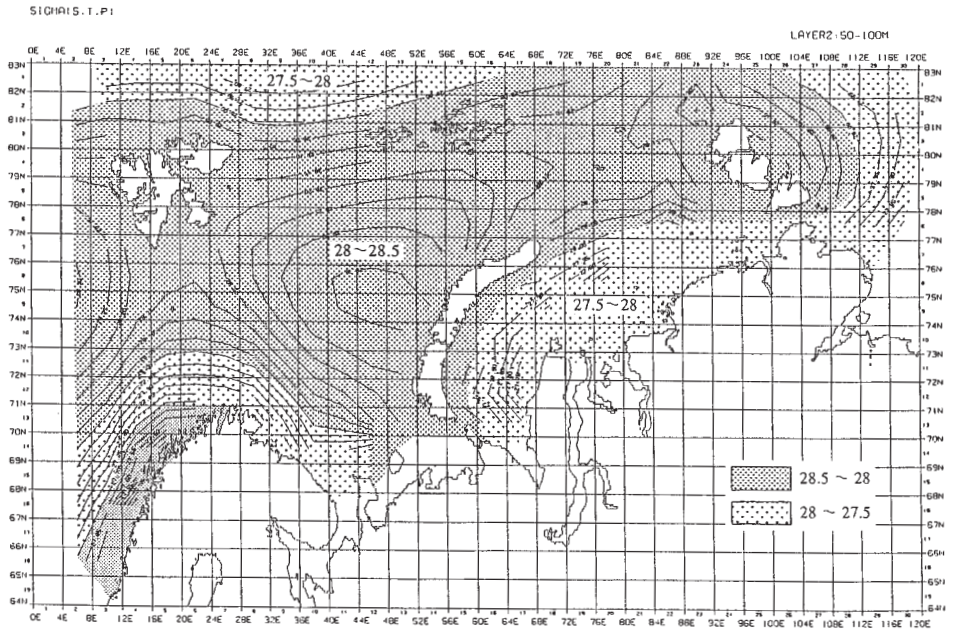

Fig. 3. (2) Density distribution σ_t (50–100m layer, warm weather season).

$4^\circ \times 1^\circ$, and each box was vertically divided into 6 layers (0～50m, 50～100m, 100～200m, 200～500m, 500～900m and 900～2500m).

Figure 2 shows the grids of the model and the number of vertical layers.

3. Oceanographic description of Arctic seawater

Density structure

Barents Sea

The Barents Sea has an area of $1.42 \times 10^6 km^2$ and volume of $3 \times 10^5 km^3$. It is largely open to the Norwegian Sea in the west and the central Arctic basin to the north. The average depth is 230m, with a maximum depth of 500m near Bear Island. The position of the Barents Sea between the Atlantic and Arctic Oceans gives it a key role to play in the transport of substances.

The Norwegian Atlantic Current which is a warm current, enters from the western side of North Cape. Then, the current is divided into two major branches. One flows eastward (coastal current system) and the other flows into the northern central area. Cold Arctic water enters from the north between Spitsbergen and Franz-Josef Land, as well as from the north between Franz-Josef Land and Novaya Zemlya (see Fig. 1). The water circulation in the Barents Sea is generally counter-clockwise (HARMS, 1992).

The Barents Sea undergoes stratification in spring and mixing in winter. This sea area is high in biological production. Salinity is 32～35 psu.

Based on the temperature and salinity distribution, density distribution maps for the layers of 0–50m and 50–100m are illustrated in Figs. 3 (1) and (2), respectively.

The density of seawater is highest in the central part of the Barents Sea and in the sea area where the Atlantic water, southwest of Spitsbergen flows north along the continental shelf, showing σ_t value of about 28. In the northernmost and southernmost parts of the Barents Sea, the density of seawater is about 0.5 lower in σ_t due to the effects of relatively light Arctic surface－layer water and coastal water, respectively.

In order to examine characteristics of water masses in the Barents and Kara Seas, T－S diagrams for each calculation box in Fig. 2 are drawn in Figs. 4 (1) and (2), respectively.

Based on the T－S diagram, surface water of the Barents Sea may be classified into four water masses as follows:

① The Atlantic water with higher temperature and higher salinity,
② The Arctic surface water with lower temperature and lower salinity,
③ The coastal water with higher temperature and lower salinity, and
④ The Barents Sea water mass that is mixture of the Atlantic water and the Arctic surface water.

By Fig. 4 (1) it can be recognized that the coastal water mixes only with the Atlantic water. The Arctic surface water first becomes more saline and then mixed with the Atlantic water, forming the Barents Sea water mass.

The density maps of Figs. 3 (1) and (2) correspond with classification of the 4 water masses, which are identified by the number in circle.

Kara Sea

The Kara Sea is $8.8 \times 10^5 km^2$ in area and $9.8 \times 10^4 km^3$ in volume. It is rather shallow; its mean water depth is 120m. However, deep valleys exist, namely, the Novaya Zemlya Trough (300～400m) east of Novaya Zemlya, and a trough (600m) north of Novaya Zemlya. In this sea area, there are inflows of river water amounting to $1{,}500 km^3$ annually, mainly from the Ob and Yenisey. These fresh water inflows cause a northward flow, forming eddies which are then branched into a northeastward－flowing current along the continent and a southwestward－flowing current along the coast of Novaya Zemlya.

River water inflows are conspicuous in summer, and decrease remarkably in winter. Figure 5 (IAEA,1998) shows monthly changes in major river water runoffs. The structure of water masses in the Kara Sea is dominated by water inflows from the Arctic Ocean and the Barents Sea as well as by river water inflows.

As was done for the Barents Sea, density distribution maps for each layer, based on the vertical distribution map of temperature and salinity for the Kara Sea, are shown in Figs. 3

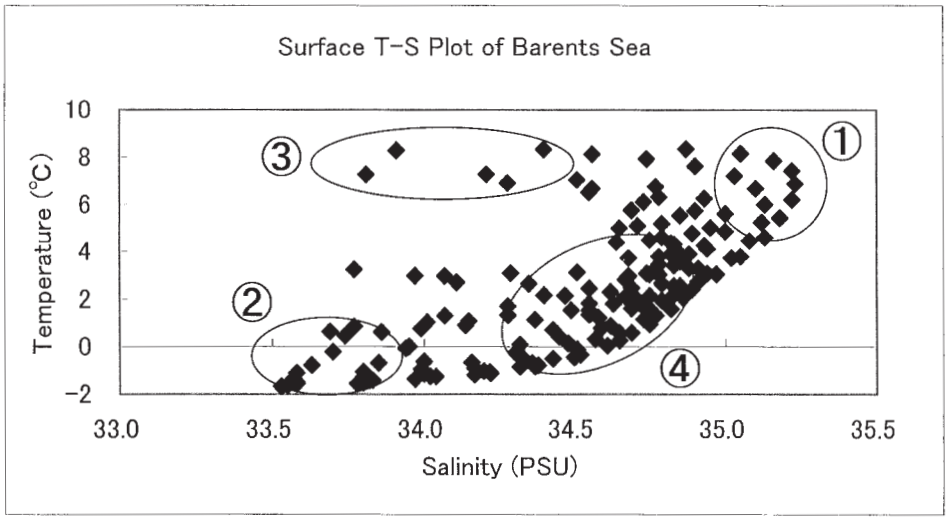

Fig. 4. (1) Surface T-S diagram of the Barents Sea.

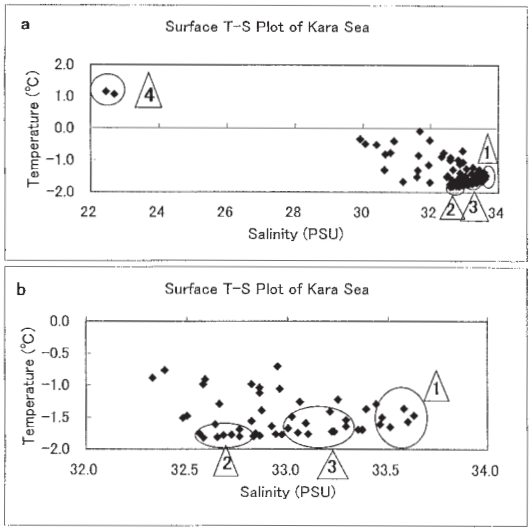

Fig. 4. (2) Surface T-S diagram of the Kara Sea.

(1) and (2). T－S diagrams were drawn also for the Kara Sea.

Fig. 4 (2)a shows total surface T－S plot of the Kara Sea, while Fig. 4 (2)b is an enlarged map of the part of salinity 32.0–34.0. From these figures, four water masses could be recognized:

⚠ The water mass characterized by higher temperature, derived from the Barents Sea,

⚠ The Arctic surface water with lower temperature and lower salinity,

⚠ The Kara Sea water mass, a mixture of the Kara Sea water and the Arctic surface water, and

⚠ The coastal water with lower salinity.

These water masses of the Kara Sea are denoted with the number in triangle in Fig. 3 (1). Salinity is 32psu offshore and 10psu near the mouths of the Ob and Yenisey river, as shown in Fig. 6.

The Barents seawater, having high density, reaches the Kara Sea with its density reduced as it advances eastward. The density of seawater in the central part of the Kara Sea becomes about 1–1.5 lower in σ_t in comparison with the Barents Sea.

The low－density water in the Kara Sea is formed by Arctic surface water entering from the north and a vast amount of fresh water entering from both the Ob river and the Yenisey river. Over the continental coast of the Kara Sea, a front is formed with density σ_t falling below 26.

Flow characteristics

LOENG *et al.* (1991) point out that the three major water masses, namely, coastal water, Atlantic water and Arctic water, are related to ocean current systems. According to Fig. 7 (LOENG *et al.* 1991), which shows the distribution of water masses in the Barents Sea, correspondence to the density distribution shown in

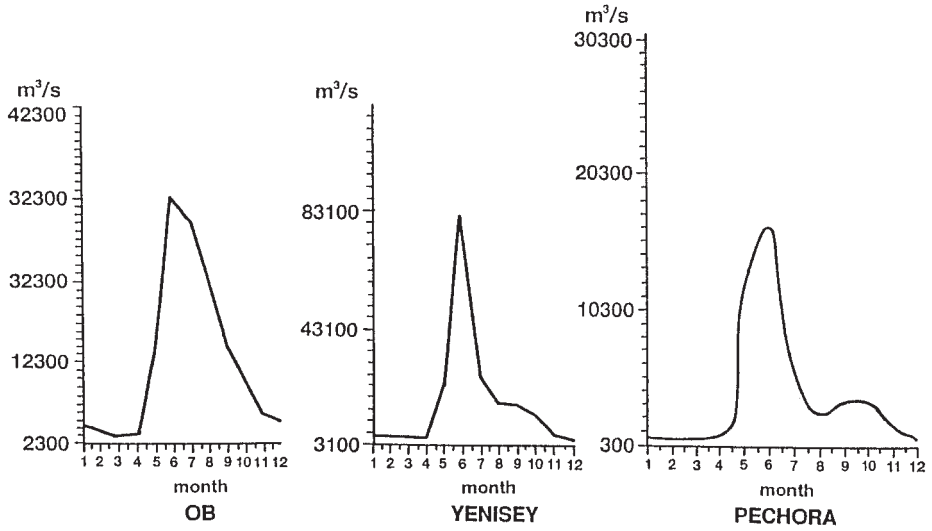

Fig. 5. Average annual cycle of river discharge to the Kara Sea and the Barents Sea (IAEA, 1998).

Fig. 3 is good.

Freezing continues for more than half of the year in this regions. The effect of wind on the flow has never been calculated. GJEVIK and STRAUME (1989) numerically calculated the tides in the North Sea, the Norwegian, Greenland and Barents Seas, and the Arctic Ocean. They concluded that in these sea areas the effect of tides is small, with the exception of coastal areas.

4. Method of flow analysis

A careful consideration must be used in the selection of an appropriate flow analysis technique for the regions having a large inflow of river water from the inland part, high－temperature and high－salinity Atlantic water masses from the western sea areas, low－temperature and high－salinity Arctic seawater from the north, large water depths and complicated topography, as seen in the Arctic Ocean.

To analyze the concentration of radionuclides extending as long as several 100 years following the flow analysis, the conservation of mass not only in each calculation box but also as a whole system must hold. That is to say, it is necessary for the following equation to hold;

$$\sum_{iB,iC}(W_{iB,iC}\ \rho_{iC}-W_{iC,iB}\ \rho_{iC})+(\text{river inflow})+\text{precipitation})-(\text{evaporation})=0$$

Where, *iB*: box number in ocean boundary, *iC*: box number in calculation box, $W_{iB,\ iC}$: exchange flow rate which enters from box *iB to box iC*, $W_{iC,\ iB}$: exchange flow rate which enters from box *iC* to box *iB*, ρ_{iC}: density of seawater in calculation box *iC*, ρ_{iB}: density of seawater in box *iB*, Σ: sum for all groups (*iB, iC*) of boundary box and calculation box.

There are two kinds of models to cope with the flow and the dispersion of radionuclides by advection and diffusion, namely compartment or box models and hydrodynamic circulation model.

Compartment or box models provide long time, spatially averaged capabilities, and some uncertainties remain in some key parameters. Hydrodynamic models provide locally resolved, short time－scale results and can only be run for limited time－scales of the order of tens of years. In the hydrodynamic models, the circulation pattern and eddy diffusivities in the model, by trial and error, are adjusted until the observed temperature and salinity distributions can be generated by the model. Moreover, there is a major shortage of quality forcing data for hydrodynamic models applied to the Arctic Ocean.

Temperature and salinity are tracers; they are the easiest of all to measure; we have much better coverage of the ocean for them than

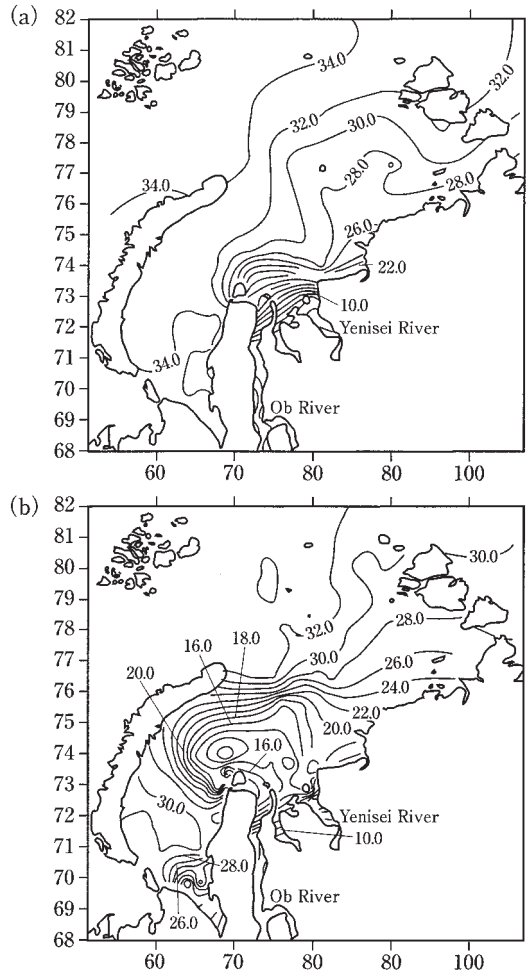

Fig. 6. Salinity distribution at the surface from data for (a) winter and (b) summer.

anything else; and their immediate relation to the density field means that they must be the central focus of any effort to understand the flow circulation. In this research, the method of analysis based on the box (compartment) model was selected because it was impossible to clearly determine the flow driving forcing in the sea areas concerned for the hydrodynamic circulation model.

Flow fields can also be generated from the observed temperature and salinity distributions in more objective ways using simplifying assumptions about the general balance of forces in the ocean interior. On the other hand, the calculation of geostrophic velocity has been used for many years in oceanography but has always suffered from the problem of not knowing what depth independent (barotropic) component of velocity needs to be added to the baroclinic results obtained (the problem of the "level of no motion"). Recently, methods of calculating the barotropic component have been derived (STOMMEL and SCHOTT, (1977); KILLWORTH, (1980)) and methods have been developed using generalized inverse techniques (WUNSCH and Minster (1982), WUNSCH (1996), EMERY and THOMASON (1998)) for calculation the flow.

For radiological assessment purposes, the use of inverse technique is particularly attractive because it does ensure that the model produced will give predictions which are comparable with observed temperature and salinity profiles in the ocean. The model used in this paper is an approach for applying conservation of mass with high accuracy not only in each calculation box also over the whole system. This model has been named a hybrid box model, intermediate one between the box model and the hydrodynamic model, developed by attending the OECD/NEA and IAEA (IASAP) modeling group meetings (IAEA Report 1998). This hybrid box model has been developed to cover the local field (Kara and Barents Seas).

5. Flow analysis by a hybrid box model

In this analysis, the flow which permits reproduction of the observed distributions of water temperature and salinity is mathematically calculated, to subsequently deal with the diffusion of nuclides.

The balance equations of seawater, salinity and heat volumes in each box are used to determine the exchange flow rate between boxes (Fig. 8).

For box i, the following are the conservation equations:

(1) Equation of conservation of seawater mass

$$\sum_{j \neq i} W_{ji}\rho_j - \sum_{j \neq i} W_{ij}\rho_i + \Sigma R_{ri}\rho_i' P_i - E_i = 0 \quad \text{[ton/s]} \quad (1)$$

Where $W_{ij} \geqq 0$: exchange flow rate from box I to box j [m^3/s], ρ_i: density of seawater in box I [ton/m^3], obtained by The International Equation of State of Seawater from water temperature and salinity, ρ_r': density of river water in

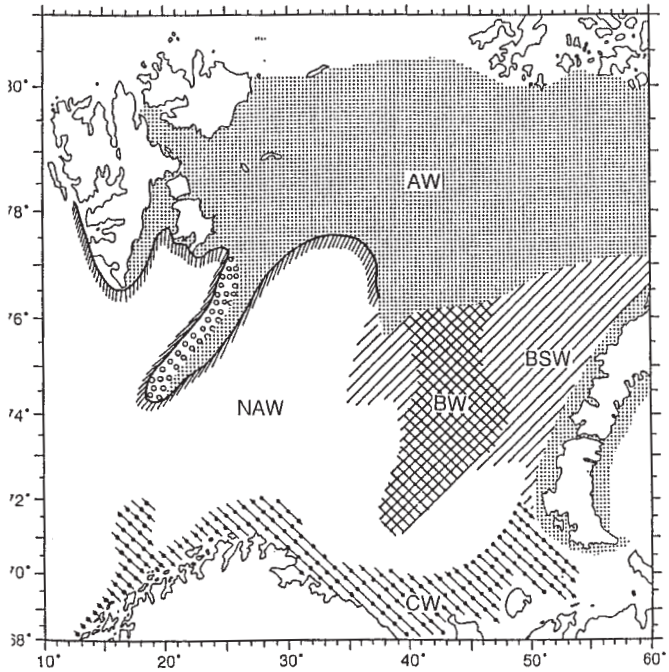

NAW : Atlantic water system
BSW : Barents Sea water system
AW : Arctic water system
BW : Bottom water system
CW : Coastal water system

Fig. 7. Distribution of water masses in the Barents Sea (LOENG *et al.*, 1991).

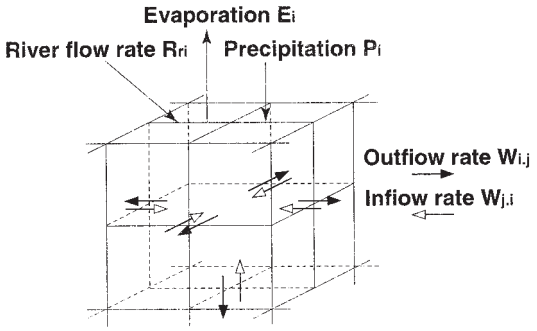

Fig. 8. Outline of the hybrid box model.

river r [ton/m^3]. R_{ri}: inflow of river water from river r to box i (m^3/s). P_i: precipitation into box i [ton/s], E_i: evaporation from box i to the atmosphere [ton/s].

The model was set up so that each exchange is represented by exchange flow rates, one in each direction. These exchange flow rates, which by definition are assumed to be positive, can be interpreted in terms of advection and mixing: to a first approximation, the mixing coefficient is the lesser of the two values and the advection is the difference.

(2) Equation of conservation of salt

$$\sum_{j \neq i} W_{ji}\rho_j S_j - \sum_{j \neq i} W_{ij}\rho_i S_i + \Sigma_r R_{ri}\rho_r'(S_i' - S_i) = 0 \quad \text{[ton/s] (2)}$$

S_i: salinity in box i [‰],
S'_i: salt in river r [‰]

(3) Equation of conservation of heat

$$\Sigma W_{ji}\rho_j T_j C - \Sigma W_{ij}\rho_i T_i C + H_i = 0 \quad \text{[Mcal/s] (3)}$$

T_i: water temperature in box i [℃], H_i: heat entering from the atmosphere into box i [Mcal/s],

C: specific heat of seawater [cal/g ℃], which is presently set at 1.0.

Although we put the terms P_i, E_i in equation (1) and the term H_i in equation (3), we did not use these terms in our calculations due to difficulties in its treatment in the surface layer. It is because the parts of these seas are largely ice－covered year－round. Therefore, the flow was analyzed using a hybrid box model, taking into account river inflows and density structures in the seas.

Table 1. Input condition of river inflow.

River	River flow rates (m^3/s)	Water temperature (℃)	Salinity (‰)
Ob	2,425.0	2.65	15.0
Yenisey	18,317.0		
Pechora	4,208.0		

Input conditions of river inflow from the river mouth are shown in Table 1.

Three equations are written in matrix form as;

$$A\underline{\boldsymbol{W}}=\boldsymbol{b} \quad (4)$$

Where A is the property matrix containing ρ, ρS and TC, $\underline{\boldsymbol{W}}$ is the vector of exchange flow rates and $\underline{\boldsymbol{b}}$ is the vector of sources and sinks.

These solutions can be expressed as the sum of a particular solution such as the least squares solution which is determined by the sources and sinks, and a series of null space solutions which are independent of the sources and sinks. So far, the least squares solution was considered to be the most useful point since it represents the flow pattern corresponding to the minimum energy in the ocean.[*1)]

Attempts using a box model have been made to use the observed temperature and salinity distributions in the Atlantic Ocean to derive a flow pattern. In conclusion, this experience with inverse techniques on the large systems such as this research showed that this has been done with the solution containing both negative and positive exchange flow rates. The difficulty in obtaining a positive solution by requiring an exact fit to the observed data is probably due to the existence of temperature and salinity gradients within the model that can only be sustained by a negative exchange flow rate. If these gradients can be removed by revising the original temperature and salinity distributions, then both a positive solution and a good fit to data my be possible.

In this model, the number of exchange flow rates, n, is less than that of equations, m, and solutions of such a problem are easily obtained either by general inverse matrix or by nonlinear programming method without constraints. However, some of exchange flow rate values thus obtained could be negative, which makes difficult to interpret the solutions as physical phenomena.

The difficulty in finding a solution was that the exchange flow rate must be non-negative (positive or 0) owing to the nature of the model. Therefore, one cannot use a simple linear equation or general inverse matrix representation and has to rely on a non-linear programming method with constraint (non-negative condition). That is to say, one does not require equations (1) to (3) to hold strictly and permits some minimizing errors.

In order to overcome this difficulty, non-negativity constraint was set for the exchange flow rate, $\underline{\boldsymbol{W}}$, ($\underline{\boldsymbol{W}}, \geqq 0$) and an efficient program was developed based on solution algorithm by mathematical formulation using a non-linear programming. This method is identical with solving a quadratic programming problem so as to minimize the objective function under the condition of non-negative exchange flow rate. That is,

Objective function (square of residual norm): $\| A\underline{\boldsymbol{W}}-\underline{\boldsymbol{b}} \|^2 \rightarrow$ min., and

Constraint: $\boldsymbol{W} \geqq 0$ (5)

Where A: m×n matrix of coefficients, determined by observation data,

$\underline{\boldsymbol{b}}$: m−dimension constant vector determined by boundary conditions,

$\underline{\boldsymbol{W}}$: n-dimensional vector of exchange flow rates,

$\| \ \|$: Euclidean norm,

m: number of conservation equations, and

n: number of exchange flow rates.

If the non-linear programming method with constraint is used, a solution can be obtained and the exchange flow rate thus obtained is non-negative, and errors in equations (1) to (3) are minimum.

[*1)] This technique is frequently employed for solving problems to obtain a fluid movement of which the total energy is restrained to be minimal, where an indefinite number of solutions can exist.

$$e = \Sigma_i \{ \alpha_1 (\text{the left side of the equation of conservation of mass (1) in box i})^2 + \beta_1 (\text{the left side of the equation of conservation of salt (2) in box i})^2 + \gamma_1 (\text{the left side of the equation of conservation of heat (3) in box i})^2 \} \quad (6)$$

Then, e is a function of the exchange flow rates W_{12}, W_{13},... and is the sum of squares of error in the conservation equations.

Exchange flow rates W_{12}, W_{13},... may be obtained under the non-negative condition W_{12}, W_{13},...> 0 to minimize the error function e = e (W_{12}, W_{13},...). This problem is usually called NNLS (Non-Negative Least Squares). Of the three equations of conservation, the unit of the first two equations is [tons/s], and that of the last equation is [Mcal/s].

Adjustment is, therefore, necessary when considering the weight of the three equations. For this adjustment, α_1, β_1 and γ_1 are set as weight constants ($\alpha_1 = 10^9$, $\beta_1 = 10^4$, $\gamma_1 = 1.0$). The values of α_1, β_1 and γ_1 above were decided by taking into consideration the agreement between results of current analysis and observation data of the Pacific Ocean and Tokyo Bay. For solution procedures to obtain the exchange flow rate, W, see Appendix I. Refer to LAWSON and HANSEN (1995) for more details.

Model validation is important. A comparison was made between literature values of water fluxes in the Arctic Ocean and values obtained from the hybrid box models. The validation process for the hybrid model has been severely restricted by the lack of appropriate flow data particularly within the Arctic area.

In the past, flow analyses were conducted in Tokyo Bay under the same input condition such as heat budget process, inflow rate of river waters, temperature and salinity distributions, using both the hybrid box model and 3D hydrodynamic model, thus confirming that there is no major difference in the results of flow circulation pattern obtained by both models (WADA *et al*., 1996).

On the other hand, the study was conducted focusing the Sea of Japan using the hybrid box model to elucidate the seasonal flow characteristics under the input conditions like inflow of Tsushima Warm Current, temperature and salinity data, heat budget process and inflow of river water from the inland area (TAKAHASHI and WADA, 1999).

The seasonal strengths of the Nearshore Branch of the Tsushima Warm Current, the East Korean Warm Current and the Liman Current were reproduced in the model. The hybrid box model was applied to the safety evaluation in a hypothetical submergence accident onto the seabed in the Pacific Ocean. Agreement was found to be good by comparison of the results of current analysis and the existing knowledge on the ocean currents (WATABE *et al*, 1996).

6. Results of flow analysis in the local field

Based on the flow velocities obtained from exchange flows in the hybrid box model, particles from each box and river mouth in the Arctic Ocean were tracked and the movement of seawater particles was studied. Particle tracking method is described in Appendix Ⅱ.

Estimation of Errors

As we search for flows which reproduce the distribution of salinity and temperature in each box, errors in salinity and heat amount can be neglected. As for flow, we calculated error of the conservation equation of seawater for each box. Errors of flow were evaluated both by the absolute error which is the difference of in and outflows and the relative error which is the difference divided by the inflow.

Table 2 shows coordinate in which the maximum error occurs (see Fig. 2), residual errors by the least square method, and the maximum value of relative error (residue/inflow) and coordinates.

Barents Sea

According to the results of tracking (Fig. 9 (1), see Appendix II), the Atlantic water which enters the Barents Sea along the Norwegian Peninsula circulates counterclockwise in the Barents Sea. This flow is in agreement with previously known data (see Figs. 10 (1) and (2)).

The results of tracking shown in Fig.9 (2) indicate that the Norwegian Atlantic current flows in from the west to the north cape. It divides into two main branches. One which flows

Table 2. Errors of conservation equation of seawater,

	Absolute error	Coordinates	Relative error	Coordinates
1st layer(0–50m)	6×10^{-4}(kton/s)	(20,4)	4×10^{-7}	(17, 13)
2nd layer(50–100m)	5×10^{-4}(kton/s)	(3,8)	4×10^{-7}	(16, 7)

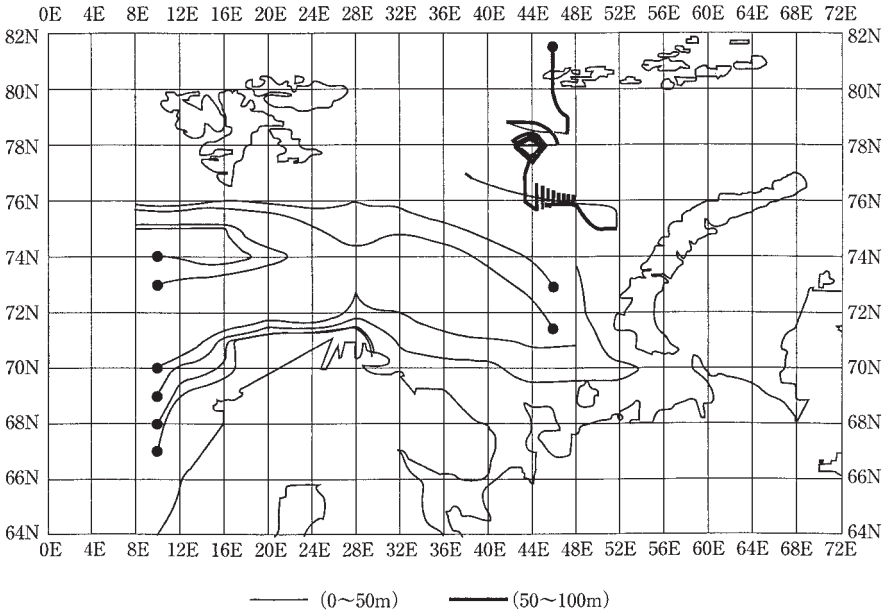

Fig. 9. (1) Result of tracking (• particle injection point).

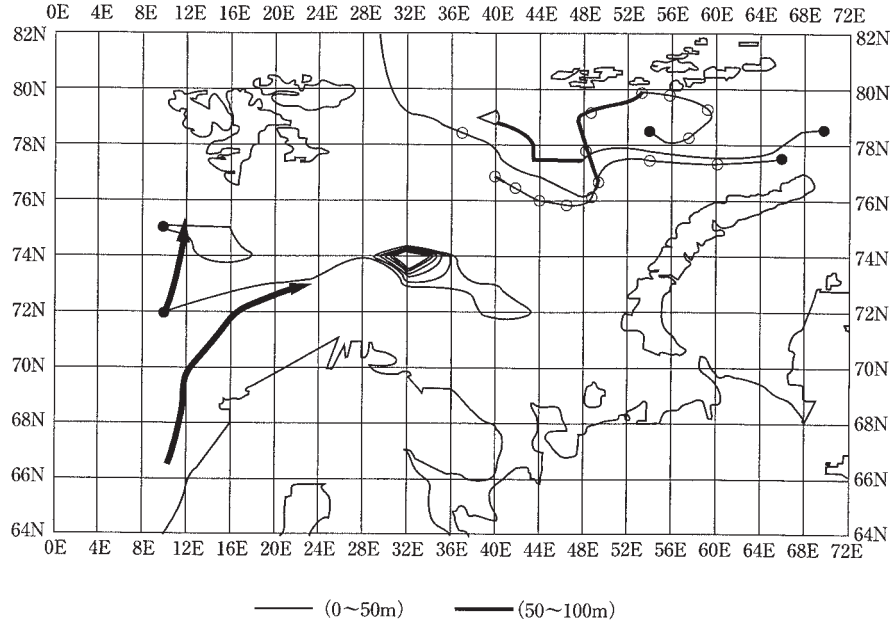

Fig. 9. (2) Result of tracking (• particle injection point).

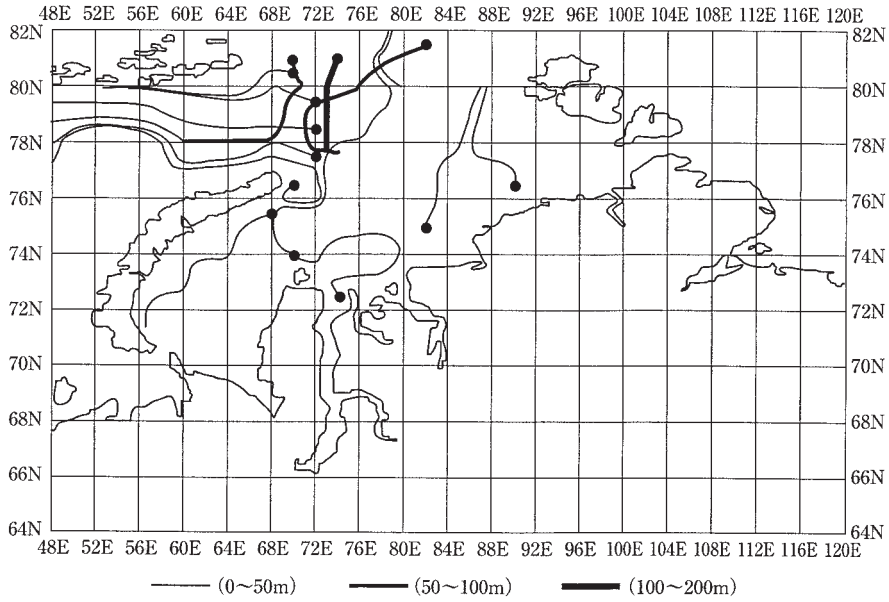

Fig. 9. (3) Result of tracking (• particle injection point).

eastward, and another which flows north.

Cold Arctic water enters from the east to the west between Franz-Josef Land and Novaya-Zemlya (Fig. 9 (2)), and from the north between Spitsbergen and Franz-Josef Land shown in Fig. 9 (1). The water circulation in the Barents Sea is generally anticlockwise judging from Figs. 9 and 10.

The current flowing southwestward at the south of Franz-Josef Land divides into two branches at the north of Sentralbanken, one of them being shown to flow southwardly toward Sentralbanken (LOENG, 1989). According to recent observations, however, this flow branch is considered to be rather minor (TANTSJURA, 1959).

As is shown in Fig. 9 (2), water particles entering from the central part of Atlantic Ocean are recognized to become gyre currents near the front shown in Fig. 10 (2).

Beween Spitsbergen and Franz-Josef Land, there exist path lines both flowing into and flowing out of the Arctic waters (Fig. 9 (1) and (2)).

Kara Sea

Fig. 11 shows schematic flow pattern in the Kara Sea (PAVLOV *et al.*, 1995). The northern sea area has a current which enters from the central Arctic Ocean along trenches of 80 to 125m deep and current which flows into the Barents Sea between Franz-Josef Land and Novaya Zemlya. The inflow from the central Arctic Sea to the Kara Sea in the second layer (50～100m) and third layer (100～200m) were reproduced successfully by tracking.

The western Kara Sea has the Novozemelskaya Current which flows from northeast to southwest along the east coast of Novaya Zemlya. The results of tracking are shown in Fig. 9 (3). This figure clearly shows that particles advance southward along the east coast of Novaya Zemlya.

The currents flowing north from the river mouths can be observed clearly.

Results and discussion

The results of flow analysis were compared with the migration routes of cod (Haddock and Barents Sea cod) to examine the reproducibility of the results. It is generally considered that Haddock cods live in 4 to 10℃ water. The sea areas which meet these conditions in the Barents Sea are the coastal area and the Atlantic water mass, with high water temperatures. The migration routes observed are shown in

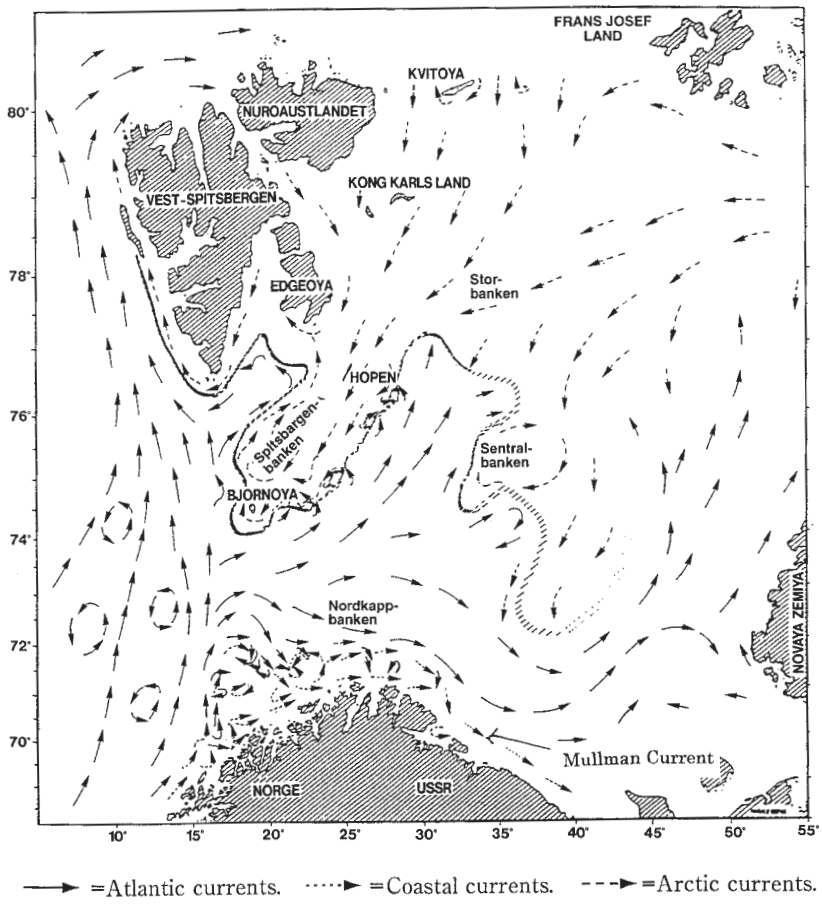

(The hatched line indicates the mean position of the Polar Front)

Fig. 10. (1) Surface -layer flow patterns in the Barents Sea (LOENG *et al.*, 1991).

Fig. 12.

The migration routes of Haddock and Barents Sea cod were compared with the results of flow analysis by the hybrid box model (Fig. 9 (1)). High similarity is recognized. In particular, the route of cods entering the Barents Sea from along the coast of Norway and migrating along the continent agrees with the tracking result. Possibly, Haddock and Barents Sea cod migrate along the Norcup Ocean Current, the Mullman Coastal Current, or the Mullman ocean current. Comparison of the model's current field with the observed surface velocity map indicate that the basic circulation pattern in the Barents Sea and the Kara Sea is captured by the model.

We also calculated the surface dynamic height from the density field and compare the result with that obtained by the particle tracks shown in Figs. 9 (1), (2) and (3). The geostrophic calculation method assumes that there is a level or depth of no motion. Level of no motion may be assumed if the currents have been measured at some depths by current meters. As we have obtained the density field from water temperature and salinity data, we calculate the flow pattern from the surface dynamic heights.

Figure 13 shows the dynamic topography at the surface layer (25m deep) of the Barents and Kara Seas in which the level of no motion is assumed to be 75m deep.

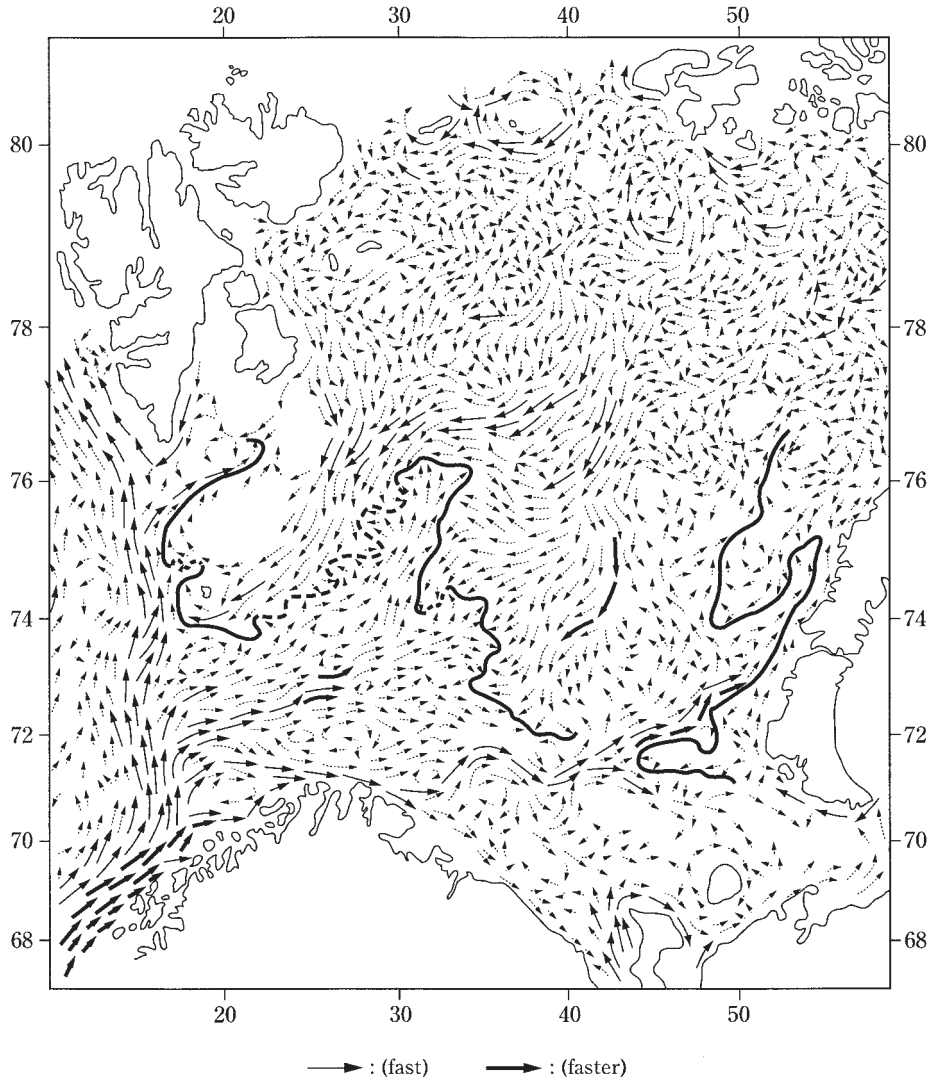

Fig. 10. (2) Scheme of the water circulation at the surface of the Barents Sea (TANTSJURA, 1959).

Following characteristics of the streamlines can be noticed:

• There exists a current which flows from east to west along the coast of the Barents Sea.

• The current turns anti-clockwise in the eastern part of the Barents Sea and flows westerly in the north of Spitzbergen Island.

• In the area between Spitzbergen Island and Novaya Zemlya, there exists a region of anti-clockwise circulation.

• In the Kara Sea, the coastal current becomes easterly under the influence of the westerly current along the coast of the Barents Sea. Consequently, a large-scale anti-clockwise circulation becomes noticeable in the region comprising the Barents and Kara Seas.

When Fig. 12 and Fig. 9 (1) and (2), which show results of the particle track, are compared, the anti−clockwise current in the Barents Sea is similar in the both cases, although

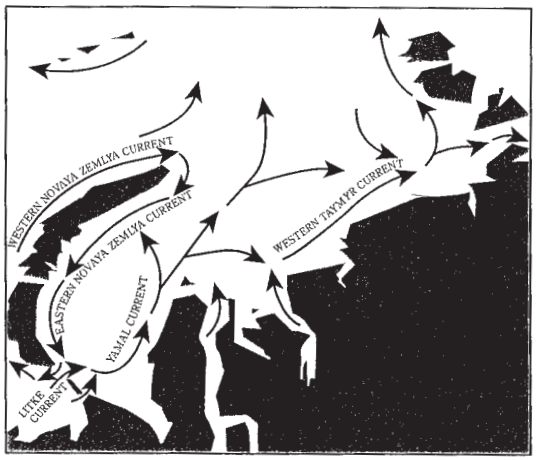

Fig. 11. Schematic flow pattern in the Kara Sea (PAVLOV *et al.*, 1995).

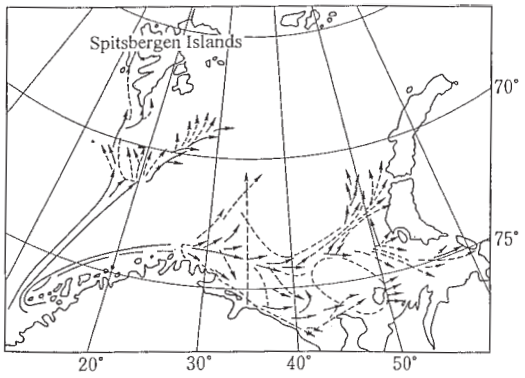

Fig. 12. Routes of the eastward migration of cods in the Barents Sea (MASLOV, 1944).
——→ Migrations of mature cod
·····→ Migrations of immature cod

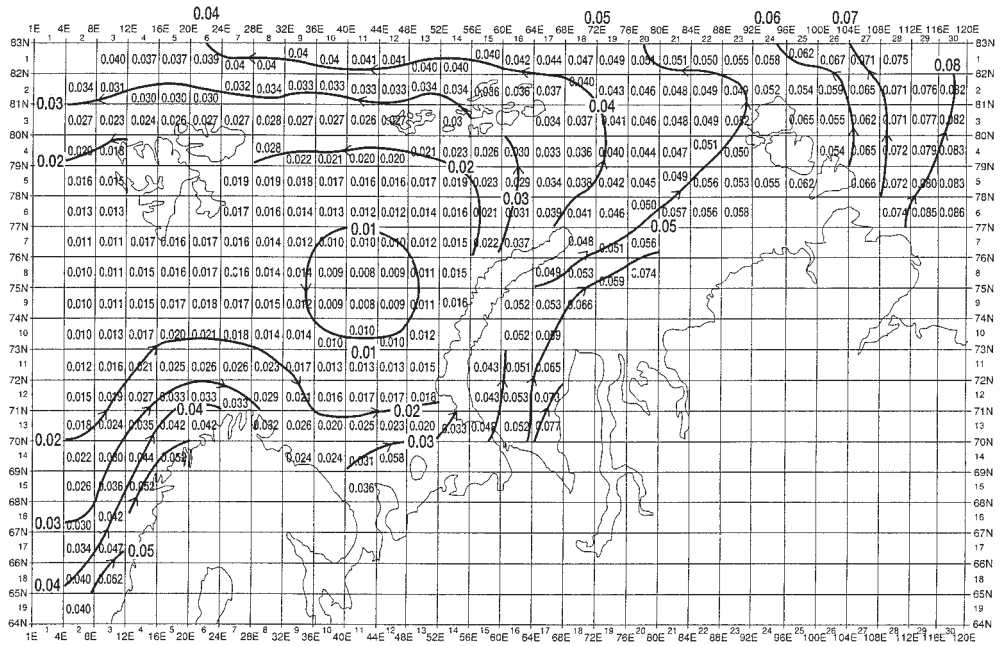

Fig. 13. Dynamic depth anomaly in the Barents Sea and Kara Sea (Unit: Dynamic meter$\times 10^{-2}$).

the anti－clockwise circulation with a small scale at the center of the Barents Sea can not be seen in the hybrid box model result.

7. Conclusions

Flow analysis was conducted by using observation data (water temperature, salinity) and applying a method for obtaining the exchange flow rate in such a way that the inter－box input and output of salinity, heat and seawater volume was balanced, and as a result,

1) Flows in the Barents Sea are affected by inflows from the neighboring seas (North Atlantic Ocean, Arctic Ocean). Inflow of river water from the Ob, Yenisey, etc. has the largest effect on changes in flows in the

Kara Sea.

2) Flows obtained with the hybrid box model agree with flows based on observed data. For the deep layers, it will be necessary to carry out further studies on the reproducibility of flows because only a small amount of Arctic deep data are available.
3) The tracking of particles was performed with respect to calculated flows. This enabled to obtain a three−dimensional movement of particles with reproducibility of high accuracy.
4) Good agreement is with migration routes of cod.

Acknowledgements

This research work was supported by the Science and Technology Agency of Japan. The authors are grateful to Mr. Teruo HOZUMI of Ark Information SYSTEM and Mr. Tairyu TAKANO and Mr. Noboru MATSUURA of Laboratory of Aquatic Science Consultant Corporation, Ltd. for their assistance in the computational work and data processing. Thanks are also due to Dr. E. ZUUR, Limnocéane, Universite de Neuchatel, who is one of the IAEA's multidisciplinary team of scientists, for his helpful advice in mathematical development in the course of carrying out this project.

References

EMERY, W. J. and R. E. THOMASON (1998): Data Analysis Methods in Physical Oceanography. Pergamon. Oxford, 634 pp.

GJEVIK, B. and T. STRAUME (1989): Model simulations of the M2 and the K1 tide in the Nordic Seas and the Arctic Ocean. Tellus. **41A**: 73 − 96.

HARMS, I. H. (1992): A numerical study of the barotropic circulation in the Barents and Kara Seas. Continental Shelf Research, **12(9)**: 1043 − 1058.

International Atomic Energy Agency (1998): Radiological Conditions of the Western Kara Sea, Report on the International Arctic Seas Assessment Project (IASAP).

KILLWORTH, P. D. (1980): On the determination of absolute velocities and density gradients in the ocean from a single hydrographic section. Deep Sea Res., **27**, 901–929

LAWSON, C. L. and R. J. HANSEN (1995): Solving Least Squares Problems. siam (Society for Industrial and Applied Mathematics), Philadelphia, Prentice-Hall, INC. 337 pp.

LEVITUS (1982): Climatorogical Atlas of the World Ocean, NOAA Professional Paper 13, National Oceanonic and Atmospheric Administration, U. S. Department of Commerce.

LOENG, H., E. SAKSHAUG, C. C. E. HOPKINS and N. ORITSLAND (1991): Features of the Physical Oceanographic Conditions of the Barents Sea. Polar Research. **10 (1)** : 5–18.

MASLOV, N. A. (1944): The bottom-fishes of the Barents Sea and their fisheries, Trudy PINRO, M.-L. YⅢ: 3–186 (in Russian).

PAVLOV, V. K. and S. L. PFIRMAN (1995): Hydrographic Structure and variability of the Kara Sea:Implications for pollutant distribution. Deep-Sea Res., **42. (6)** : 1369− 1390.

STOMMEL, H. and SCHOTT, F. (1977): The beta spiral and the determination of the absolute velocity field from hydrographic station data. Deep Sea Res., **24,** 325–329.

TAKAHASHI, Y. and A. WADA (1999): Study on Flow in the Sea of Japan by Box Model. Journal of Hydroscience and Hydraulic Engineering, JSCE. **17** (2): 139–158.

TANTSJURA, A. (1959): About the current of the Barents Sea, Proc. PINRO, **11**, 35–53 (in Russian)

VOLKOV, V. A., O. JOHANNESSEN, V. E. BORODACHEV, G. N. VOINOV, L. H. PETTERSSON, L. P. BODYLEV and A. V. KOURAEV (2002): Polar Seas Oceanography, An integrated case study of the Kara Sea, Chichester, UK, Praxis Publishing, 450pp.

WADA, A., T. TAKANO and T. HOZUMI (1996): Estimation method for Residence Time of Bay Water. Journal of Hydroscience and Hydraulic Engineering, JSCE, **14** (1): 57–66.

WADA, A., Y. KINEHARA and T. TAKANO (1997): Marine contamination in the Arctic Ocean. J. of Global Environmental Engineering. JSCE. **3**: 37–51.

WATABE, N., Y. KOHNO, D. TSUMUNE, T. SAEGUSA and H. OHNUMA (1996): An Environmental Impact Assessment for Sea Transport of High Level Radioactive Waste. RAMTRAN, **7** (2/3):117–127

WUNSCH, C. (1996): The Ocean Circulation Inverse Problem. Cambridge University Press. Cambridge, 442 pp.

WUNSCH and MINSTER (1982): Methods for box

models and ocean circulation tracers: Mathematical programming and non-linear inverse theory, J. Geophys. Res., **87**, 5647–5662.

Appendix I

Solving method for the hybrid box model

Solution of obtaining the exchange flow rates by means of a compartment model is identical with solving a quadratic programming problem so as to minimize the objective function under the condition of non-negativity of exchange flow rate, $\boldsymbol{W}$. That is,

Objective function (square of residual norm): $\| A\boldsymbol{W}-\boldsymbol{b} \|^2$, and Constraint: $\boldsymbol{W} \geq 0$,

where A: m n matrix of coefficients, determined by observation data,

$\boldsymbol{b}$: m-dimension constant vector determined by boundary conditions,

$\boldsymbol{W}$: n-dimension vector of exchange flow rates,

$\| \cdot \|$: Euclidean norm,

m: number of conservation equations, and

n: number of exchange flow rates.

Mathematically, this problem is called convex quadratic programming problem or NNLS (Non Negative Least Squares).

Solution processes

Algorithm of the active set method is premised on three points as follows:

1) When all of exchange flow rates are 0, it satisfies the equations and constraint,
2) Solution of quadratic programming problem without constraint can be obtained by the usual least squares method, and
3) Criteria of optimum solution are given by the Kuhn－Tucker's condition that is usually applied in quadratic programming method.

Outline of the algorithm for obtaining optimum solution is summarized as follows:

① First, let all elements of exchange flow rate be 0, and select an element Wq that leads to the optimum solution most closely;
② Solve the quadratic programming problem without constraint, and correct the resulting solution so as to fulfill the non-negativity restraint;
③ Using the corrected solution, solve again quadratic programming problem without constraint, and correct solution that does not satisfy the non-negativity constraint; and
④ When the non-negativity constraint is fulfilled, select another element of exchange flow rate that has been set to be 0, and repeat the procedures above, thus decreasing one by one the number of elements set to be 0, until the optimum solution is reached.

Appendix II

Particle Tracking Method in Arctic Sea Box Model

1. Particle Tracking Method Particle tracking is defined here as positioning of a particle from a given initial position in a given flow field after an arbitrary time elapsed. Equations representing a particle tracking movement in the spherical coordinates are:

$$\dot{\lambda} = \frac{u}{r\cos\varphi}$$

$$\dot{\varphi} = \frac{v}{r}$$

$$\dot{r} = w,$$

where u: longitudinal flow rate component (m/s), v: latitudinal flow rate component (m/s), and w: vertical flow rate component, each being function of:longitude,: latitude, and r: vertical coordinate (distance from the geocenter, respectively. The mark " • " denotes the temporal differential.

One of the typical solutions for such equations is the (explicit) Eulerian solution, Δt being the time interval:

$$\lambda^{n+1} = \lambda^n + \Delta t \frac{u(\lambda^n,\ \varphi^n,\ r^n)}{r^n \cos\varphi^n}$$

$$\varphi^{n+1} = \varphi^n + \Delta t \frac{v(\lambda^n,\ \varphi^n,\ r^n)}{r^n}$$

$$r^{n+1} = r^n + \Delta t w(\lambda^n,\ \varphi^n,\ r^n) \qquad (\mathrm{A\,II} \cdot 2)$$

in which the position at time $n\Delta t$ is approximated as $(\lambda n,\ \varphi n,\ rn) \approx (\lambda\ (n\Delta t),\ \phi\ (n\Delta t),\ r\ (n\Delta t)$.

In solving the Eq. (A II • 2) using a computer, we must decide the flow field

$$\left(\frac{u(\lambda^n,\ \varphi^n,\ r^n)}{r^n\cos\varphi^n},\ \frac{v(\lambda^n,\ \varphi^n,\ r^n)}{r^n},\ w^n\right)$$

Since the flow field given by Arctic Sea Box

Model is defined only at discrete positions, flow field at an arbitrary position needs to be

obtained by interpolation.

2. Interpolation of Flow Rate

Processes in the particle tracking program "stm. f" are as follows:

1) Dimensions of the left-and right-hand members of Eq. (A Ⅱ • 1) are matched, that is to say, the flow field (u, v, w) is transformed into the flow field (u, v, w):

$$\dot{\lambda} = u,\ u = \frac{u}{r\cos\varphi},$$

$$\dot{\varphi} = v,\ v = \frac{v}{r}$$

$$\dot{r} = v,\ w = w, \qquad (\text{A Ⅱ} \cdot 3)$$

in which the dimension of flow rate in the longitude latitudinal equations is angle per unit time.

2) Obtain the flow field (u, v, w) at an arbitrary position by means of multilinear interpolation (three－dimensional bilinear interpolation; see appendix "Basis of Interpolation").

Received April, 5, 2002
Accepted November, 17, 2003